Parameter identification of a fractional-order human-exoskeleton coupling model with the segmented form for the lower limb

1st Zhenlei Chen
School of Automation Engineering
University of Electronic Science and Technology of China
Chengdu, China
zhenlei_chen@std.uestc.edu.cn

2nd Tieshan Li
School of Automation Engineering
University of Electronic Science and Technology of China
Chengdu, China
tieshanli@126.com

3rd Yao Yan
School of Aeronautics and Astronautics
University of Electronic Science and Technology of China
Chengdu, China
y.yan@uestc.edu.cn

4rd Qing Guo
School of Aeronautics and Astronautics
University of Electronic Science and Technology of China
Chengdu, China
guoqinguestc@uestc.edu.cn

***Abstract*—This paper presents a novel human-exoskeleton coupling model for estimating human-exoskeleton coupling force. To enhance the model's ability to characterize the complex mechanical characteristics of human-exoskeleton coupling, the fractional-order differential term is introduced. Furthermore, the coupling model adopts the segmented form to characterize the different mechanical characteristics of the front and back sides of the human-exoskeleton coupling point. Using experimental data measured by the self-developed human-exoskeleton coupling measurement platform, the corresponding model parameters for 10 adult male and 10 adult female volunteers (Age: 23.65 $\pm$ 4.03 years, Height: 165.60 $\pm$ 8.32 cm, Weight: 62.35 $\pm$ 14.09 kg) were identified via Neighborhood Field Optimization (NFO) and Least Squares (LS) methods. Based on the analysis of the estimated root mean square error (RMSE) of the coupling force, it can be verified that the coupling force can be estimated accurately based on the proposed fractional-order human-exoskeleton coupling model with the segmented form.**

***Index Terms*—Human-exoskeleton coupling model, Fractional-order differential term, Segmented form, Model parameter identification**

I. Introduction

The exoskeleton is employed to facilitate human rehabilitation, strength augmentation, or locomotion assistance, combining human wisdom and robotic strength. Since 2000, exoskeleton technology has experienced rapid development, with several notable exoskeleton prototypes being designed, such as C-ALEX [1] and LOPES [2] for rehabilitation, HULC [3] and BLEEX [4] for strength augmentation, and ReWalk [5] and HAL [6] for locomotion assistance. The control mode of an exoskeleton can generally be classified into two groups: passive mode and active mode. An exoskeleton with passive mode drives the wearer to track the pre-generated desired trajectories [7], which are obtained from measurements of a healthy subject or designed by a professional sports planner. In active mode, the actual trajectory of the exoskeleton is adjusted in accordance with the wearer's motion intention [8]. Specifically for the position control of the exoskeleton, a variety of control algorithms are currently being studied, such as proportional-integral-derivative, fuzzy, adaptive, sliding-mode controllers [9]–[11].

To ensure the performance of human-exoskeleton coupling motion, it is necessary to investigate the motion characteristics of the human body. In recent years, some research has been conducted on the mechanical characteristic of human limbs in motion, including upper and lower limbs [12], [13]. Ma *et al*. [14] proposed an estimation model for the endpoint stiffness of the human arm from electromyographic signal (sEMG) and elbow angle. Liu *et al*. [15] combined muscle activation and muscle contraction dynamics to identify upper limb stiffness. For the limb-connected exoskeleton, to accurately perceive or estimate the wearer's motion intention, it is necessary to establish an accurate human-exoskeleton coupling model and identify its parameters. Yan *et al*. [16], [17] proposed a simple linear damping-spring human-exoskeleton coupling model, and the model parameters were identified through physical coupling experiments. Huang *et al*. [18] proposed a complex nonlinear human-exoskeleton coupling model for predicting human-exoskeleton coupling forces. This study aims to introduce the fractional-order differential term to enhance the capability to characterize the mechanical characteristic of human-exoskeleton coupling, and to utilize the segmented form for the asymmetry of human-exoskeleton coupling. The

This research is supported by National Natural Science Foundation of China (Grants No. 52305054, 51939001, 12072068, and 52175046), National Natural Science Foundation of Sichuan (Grant No. 2024NSFSC1479), China Postdoctoral Science Foundation (Grant No. 2022M720024), and Sichuan Science and Technology Program (Grant No. 24ZDYF0070). (Corresponding authors:Tieshan Li.)

fractional order calculus has been successfully utilized in modeling viscoelastic materials [19]. Specifically, Aydin *et al*. [20] proposed a fractional order admittance controller for physical human-robot interaction motion.

The current human-exoskeleton coupling model exhibits issues pertaining to low accuracy or a complex form. A novel fractional-order human-exoskeleton coupling model with segmented form is proposed, and the main contributions are as follows:

(1) The fractional-order differential term is introduced to enhance the capability to characterize the mechanical characteristics of human-exoskeleton coupling. Furthermore, the segmented form is employed to characterize the mechanical characteristics in different human-exoskeleton coupling states (front-side compression or back-side compression).

(2) A human-exoskeleton coupling model parameter identification method based on the NFO and LS is proposed. The coupling model parameters of 20 volunteers were identified under different coupling positions and levels of looseness. To verify the accuracy of the proposed human-exoskeleton coupling model and the effectiveness of the parameter identification method, the RMSE of the coupling force was analyzed.

Since human body motion primarily occurs in the sagittal plane, and this study focuses on the human-exoskeleton coupling normal force resulting from the lateral tension or compression of the soft human-exoskeleton coupling, only the human-exoskeleton coupling model in the X-axis is considered. This means that the coupling force and relative displacement mentioned in the following text refer specifically to the components in the X-axis (see Fig. 1).

The remainder of this paper is structured as follows. Section II introduces the self-designed human-exoskeleton coupling measurement platform and fractional order calculus. Section III describes the fractional-order human-exoskeleton coupling model with the segmented form and outlines the model parameter identification method. Section IV presents the results of the model parameter identification for 20 volunteers. Finally, conclusions are drawn in Section V.

II. Plant and Preliminary

A. Human-exoskeleton Coupling Measurement Platform

For the purpose of identifying the parameters of the human-exoskeleton coupling model, it is imperative to accurately collect and record the motion displacement of human and coupling force during the human-exoskeleton coupling motion. Hence, we developed the human-exoskeleton coupling measurement platform shown in Figs. 2-3. The main structure of the device is a stainless steel rigid frame, which is considered an analog for the lower-limb exoskeleton. A three-dimensional (3D) force sensor (LH-SZ-02-100) and two laser displacement sensors (ILD1420-200) are employed, and the measured data is recorded at a sampling frequency of 15625 Hz and transferred to NI-DAQ Express using the NI USB-6210 device. Then, the actual measured data is filtered using a Butterworth digital filter (cutoff frequency:10 Hz) to remove measurement noise. Additionally, the position of these sensors

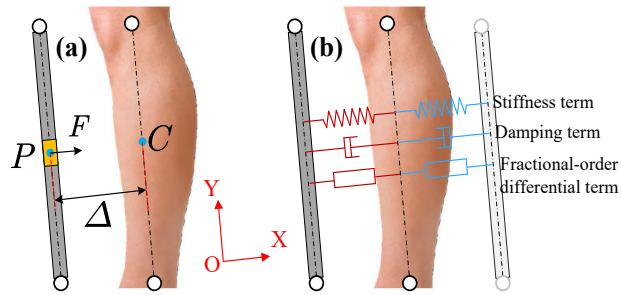

Fig. 1. The schematic diagram of human-exoskeleton coupling motion:(a) relative displacement Δ and coupling force F at the coupling point, (b) the fractional-order human-exoskeleton coupling model with the segmented form.

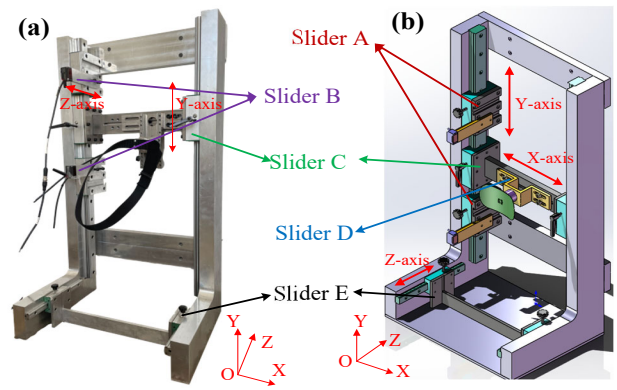

Fig. 2. The mechanical structure of the human-exoskeleton coupling measurement platform: (a) the photo, (b) the 3D design.

can be adjusted by moving the slider, allowing for adaptation to different volunteers. For instance, Sliders C and D facilitate the adjustment of the force sensor in the Y and X-directions, while the laser sensors can be moved along the Y and Z-directions by adjusting Sliders A and B, respectively.

B. Fractional Order Calculus

Fractional order calculus is a generalization of integer order calculus, which allows integration and differentiation of non-integer orders. Several definitions exist for the fractional-order differintegral operator, including the Grunwald-Letnikov, Riemann-Liouville, and Caputo definitions.

In this study, we use the Simulink module from the FOMCON toolbox in Matlab/Simulink to perform fractional order derivative calculations. Then, a fractional-order human-exoskeleton coupling model with the segmented form is proposed to characterize the coupling characteristic between human and exoskeleton.

III. Methods

A. Human-exoskeleton Coupling Model

In the human-exoskeleton coupling collaborative task, the operator's lower limbs and the exoskeleton are bundled and connected using belts or other devices. The rigid exoskeleton, constructed from metal or composite materials, is a typical rigid body. Similarly, the human skeleton, with an elasticity

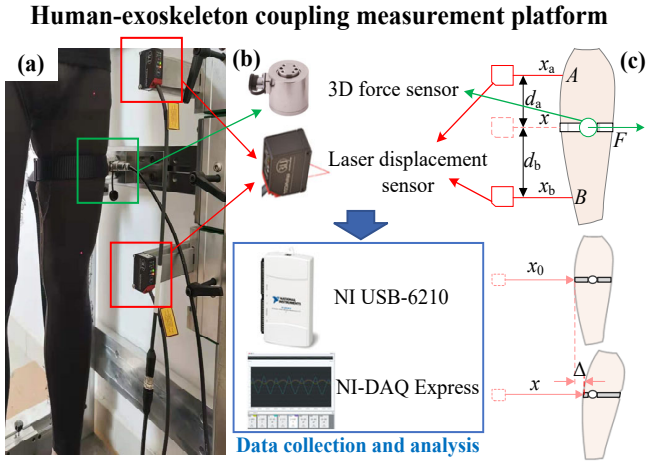

Fig. 3. The schematic diagram of the human-exoskeleton coupling measurement platform:(a) the actual experimental scene, (b) sensors, data collection and analysis system, (c) calculation and measurement methods for the human-exoskeleton coupling relative displacement Δ and the coupling force F.

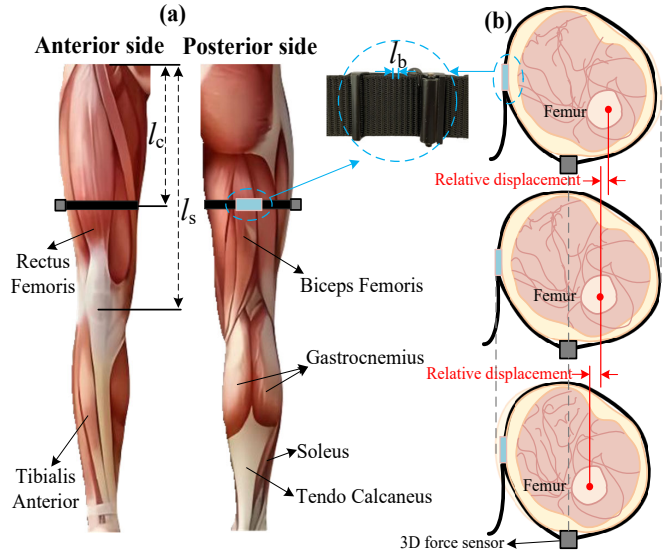

Fig. 4. (a) Anterior and posterior muscle distribution of the human lower limb, (b) Top view of the coupling position between the human and the exoskeleton in three cases: front-side compression, human-exoskeleton synchronization, and back-side compression.

modulus ranging from 12 to 20 GPa [21], can also be regarded as a rigid body. The human-exoskeleton relative motion leads to tension or compression of the soft human-exoskeleton coupling, including belt, skin, muscle, and fat, resulting in the human-exoskeleton coupling force. Therefore, in order to accurately infer or estimate the operator's motion intention based on the real-time coupling force, it is necessary to construct a sufficiently accurate human-exoskeleton coupling model.

As depicted in Fig. 1-(a), the relative motion between the coupling points P on the exoskeleton and C on the human leg results in the generation of the coupling force F. A simple stiffness-damping model for F can be expressed as

$$F = b_{sd}\dot{\Delta} + k_{sd}\Delta, \tag{1}$$

where $\dot{\Delta}$ and Δ are the relative velocity and displacement at the human-exoskeleton coupling point, and b_{sd} and k_{sd} are the coupling damping and stiffness.

However, based on the following two considerations, it is challenging to accurately characterize the actual human-exoskeleton coupling characteristic using (1).

1) Complex mechanical characteristics of human-exoskeleton coupling: The actual human-exoskeleton coupling is composed of textile fabrics, including belt and pants, as well as human soft tissues, such as the fat layer, muscle tissue, and skin tissue of the human lower limb. As a result, it exhibits complex mechanical characteristics, such as viscoelasticity.

2) Asymmetry of human-exoskeleton coupling: As shown in Fig. 4, the relative motion between the human lower limb and the exoskeleton results in the generation of human-exoskeleton coupling force, which is attributed to compression, stretching, friction, and other phenomena occurring at the human-exoskeleton coupling. There is a distinct difference in the soft tissue on the front and back sides of the human leg, such as muscle distribution (Fig. 4-(b)) and fat thickness. Therefore, there is a significant difference in the mechanical characteristics of human-exoskeleton coupling between the two cases of front-side compression and back-side compression. In summary, there is a notable asymmetry in the mechanical characteristics of human-exoskeleton coupling.

Based on the aforementioned analysis, a fractional-order human-exoskeleton coupling model with the segmented form is constructed, which is expressed as follows:

$$F = \begin{cases} b_{sfd-p}\dot{\Delta} + c_{sfd-p}\mathscr{D}^{\alpha}\Delta + k_{sfd-p}\Delta, & \Delta > 0 \\ b_{sfd-n}\dot{\Delta} + c_{sfd-n}\mathscr{D}^{\alpha}\Delta + k_{sfd-n}\Delta, & \Delta \leq 0 \end{cases}, \tag{2}$$

where b_{sfd-i} and k_{sfd-i} $(i = n, p)$ are the coupling damping and stiffness, $\mathscr{D}^{\alpha}\Delta$ is the α-order differintegral of Δ with $\alpha \in (0, 1)$, and c_{sfd-i} $(i = n, p)$ is the coefficient of $\mathscr{D}^{\alpha}\Delta$. Generally, α is a pre-designed parameter, and it is set to 0.5 in this study.

Compared to the stiffness-damping model (1), the proposed coupling model (2) employs a segmented form, which uses corresponding model parameters (b_{sfd-i}, k_{sfd-i}, c_{sfd-i}, $i = n, p$) to characterize the mechanical characteristics in different human-exoskeleton coupling states (front-side compression $\Delta \leq 0$ or back-side compression $\Delta > 0$). Additionally, the fractional-order differential term $c_{sfd-i}\mathscr{D}^{\alpha}\Delta$ $(i = n, p)$ is introduced to enhance the capability to characterize the mechanical characteristic of human-exoskeleton coupling.

B. Parameter Identification of Coupling Model

During the human-exoskeleton coupling motion experiment, the volunteers were secured to the human-exoskeleton coupling measurement platform, yielding relative movement and coupling force. Furthermore, due to the flexibility of human-exoskeleton coupling, there exists local tissue deformation

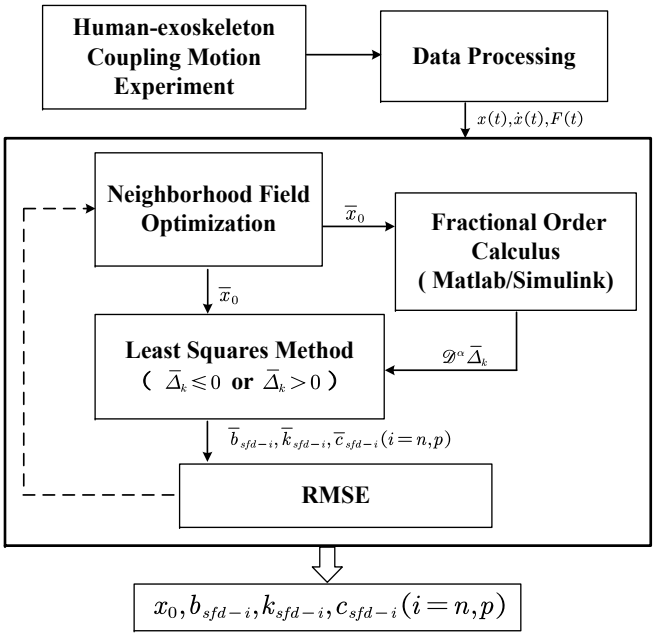

Fig. 5. The parameter identification flow chart of the fractional-order human-exoskeleton coupling model with the segmented form (2).

at the coupling point, which implies that the horizontal displacement of the coupling point cannot be directly measured. As shown in Fig. 3-(c), two independent laser sensors are employed to measure the horizontal displacements $x_a(t)$ and $x_b(t)$ of the measurement points A and B, respectively. An indirect method for calculating relative displacement $\Delta(t)$ is adopted at time t, which can be expressed as

$$\Delta(t) = x(t) - x_0, \quad x(t) = \frac{x_b(t)d_a + x_a(t)d_b}{d_a + d_b}, \tag{3}$$

where $x(t)$ is the horizontal displacement between the coupling point and the connection line of the dual laser sensors, and x_0 is the constant displacement for zero coupling force.

Actually, volunteers vary in leg shape, and their standing positions also differ across group experiments. Even within a single group experiment, the standing position of volunteers may slightly change. Hence, accurately measuring x_0 is difficult. In this study, x_0 is also considered a parameter to be identified, similar to b_{sfd-i}, k_{sfd-i}, and c_{sfd-i} $(i = n, p)$.

During the experiment, a series of data regarding the variables x and F were obtained, as follows:

$$\begin{cases} x_k = x(k \times \Delta t), k = 1, 2, 3, \ldots, k_{\max} \\ F_k = F(k \times \Delta t), k = 1, 2, 3, \ldots, k_{\max} \end{cases}. \tag{4}$$

To balance accuracy and computational efficiency, the original data sequence was uniformly sampled at a ratio of $1:10$ prior to performing parameter identification. Hence, the actual sampling period $\Delta t = \frac{2}{3125}$s, and $k_{\max} = 93125$. The velocity used in parameter identification was approximately obtained by the backward difference method.

As shown in Fig. 5, during the process of parameter identification, the NFO algorithm is employed to optimize x_0, where NFO is a heuristic algorithm inspired by the interplay of gravitational attraction and repulsion among natural particles and their neighbors. In the NFO algorithm, when an individual adopts the x_0 value $\bar{x}_0$ in the optimization process (where $\bar{\bullet}$ represents the calculated value of $\bullet$ for an individual in a particular process), the corresponding fractional differential sequence $\mathscr{D}^\alpha \bar{\Delta}_k$ is calculated using Matlab/Simulink. Then, to ensure the stability of $\mathscr{D}^\alpha \bar{\Delta}_k$, the first $k_{\min} = 19999$ data points in all data sequences, including $\mathscr{D}^\alpha \bar{\Delta}_k$, Δ_k, $\dot{\Delta}_k$, and F_k, are ignored. Based on the value of $\bar{\Delta}_k$ ($\bar{\Delta}_k \leq 0$ or $\bar{\Delta}_k > 0$), the data are divided into two groups to identify model parameters $\bar{b}_{sfd-i}$, $\bar{k}_{sfd-i}$, and $\bar{c}_{sfd-i} (i = n, p)$ using the LS method. The corresponding estimated coupling force sequence $\bar{F}_k^{\text{fit}}$ is calculated according to (2). The optimization object of NFO is set as $\min \text{RMSE}(F_k, \bar{F}_k^{\text{fit}})$, where $\text{RMSE}(F_k, \bar{F}_k^{\text{fit}})$ is defined as

$$\text{RMSE}(F_k, \bar{F}_k^{\text{fit}}) = \sqrt{\frac{1}{k_{\max} - k_{\min}} \sum_{j=k_{\min}+1}^{k_{\max}} (\bar{F}_{k,j}^{\text{fit}} - F_{k,j})^2}. \tag{5}$$

where $F_{k,j}$ and $\bar{F}_{k,j}^{\text{fit}}$ are the j-th elements of the data series F_k and $\bar{F}_k^{\text{fit}}$, respectively. When the NFO algorithm reaches the termination condition, the optimization value of x_0 and the corresponding parametes b_{sfd-i}, k_{sfd-i}, and c_{sfd-i} $(i = n, p)$ are the parameter identification results.

C. Coupling Position and Looseness

For this study, a total of 20 adult volunteers, consisting of 10 males and 10 females with varying body types (Age: 23.65 ± 4.03 years, Height: 165.60 ± 8.32 cm, Weight: 62.35 ± 14.09 kg), were recruited. The volunteers operated the platform with the human-exoskeleton coupling position and tightness as control variables.

As shown in Fig. 4-(a), considering differences in leg length among volunteers, a length ratio l_p is used to represent the coupling position and is defined as

$$l_p = \frac{l_c}{l_s} \times 100\%, \tag{6}$$

where l_c is the vertical distance from the proximal end of each segment to the coupling position, and l_s is the segment length.

Similarly, the leg circumference at the coupling position also exhibits significant differences. As shown in Fig. 4, the canvas belt has evenly distributed teeth with an interval of l_b, and the coupling tightness can be adjusted by maneuvering and securing the box-frame buckle into place.

For the initial test of each volunteer, the belt was tightened to the maximum extent that the volunteer could tolerate. Subsequently, for every subsequent test, the coupling was loosened by 2 teeth. Therefore, the releasing length of the belt is used to quantify the degree of looseness, and the looseness $L_{\text{looseness}}$ is defined as

$$L_{\text{looseness}} = l_b n_s, \tag{7}$$

where n_s is the number of buckle slots to be loosened, and $l_b = 3.53$ mm.

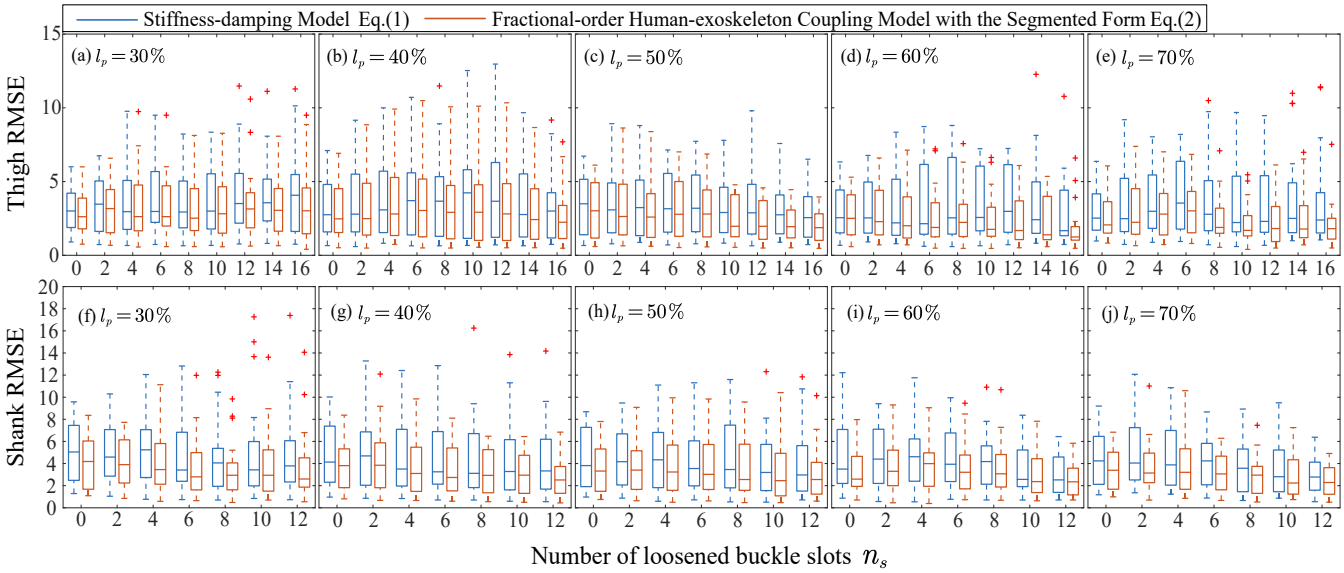

Fig. 6. The RMSE of the human-exoskeleton coupling force based on stiffness-damping model (1) and the fractional-order human-exoskeleton coupling model with the segmented form (2). The level of looseness indicated on the horizontal axis is represented by the number of belt slots loosened by the buckle n_s.

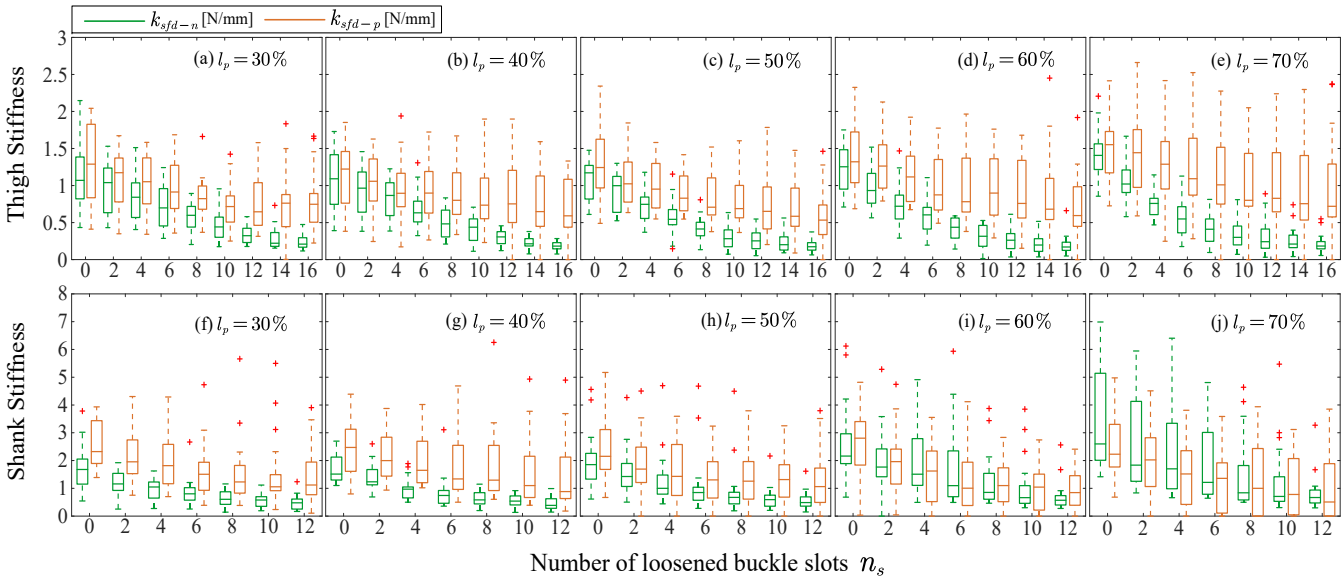

Fig. 7. The human-exoskeleton coupling stiffness parameters k_{sfd-n} and k_{sfd-p}. The level of looseness indicated on the horizontal axis is represented by the number of belt slots loosened by the buckle n_s.

IV. Results and Discussion

For each volunteer, the coupling position parameters were identified for l_p values of $70\%, 60\%, 50\%, 40\%$, and 30%. Subsequently, the belt was gradually loosened to achieve 9 and 7 levels of tightness in the thigh and shank, respectively. Thus, there are 45 and 35 groups of data for identifying thigh- and shank-exoskeleton coupling model parameters for every volunteer, with the fractional order $\alpha = 0.5$.

In this section, the boxplot is adopted to illustrate the statistical results, where outliers are identified as data points that lie away from the median, 1.5 times larger than the interquartile range, which is defined as the range between the 25th and 75th percentiles of the data. As shown in Fig. 6, based on the stiffness-damping model (1) and the fractional-order coupling model with the segmented form (2), each boxplot indicates the distribution of RMSE of the force-fitted among 20 volunteers at a particular coupling position l_p and with the same level of coupling looseness. For comparison, the prediction of human-exoskeleton coupling force by the proposed fractional-order coupling model with the segmented form (see (2)) exhibits significantly better accuracy and a more concentrated distribution.

Given that elasticity is the most explicit mechanical characteristic of human-exoskeleton coupling, we specifically analyzed the identified stiffness coefficient k_{sfd-n} and k_{sfd-p}. Fig. 7 presents the influence of coupling looseness on the stiffness in two human-exoskeleton coupling states ($\Delta \leq 0$ or $\Delta > 0$), k_{sfd-n} and k_{sfd-p}, across 10 different coupling positions. Regardless of the coupling position l_p, the stiffness values k_{sfd-n} and k_{sfd-p} always decrease as the looseness increases. In particular, due to the increased difficulty in maintaining balance when the leg is leaning backward compared to when it is leaning forward during the experiment, volunteers may exhibit a lack of data specifically in cases involving backward leg leaning in certain experiments. Furthermore, under the same coupling position l_p and looseness, the value of k_{sfd-p} is generally larger than that of k_{sfd-n}. When $\Delta > 0$, this indicates that there is a squeeze between the back side of the human leg and the belt. Conversely, when $\Delta \leq 0$, it signifies that the front side of the human leg is squeezed by the belt. As shown in Fig. 4, whether it is the thigh or shank of the human body, the posterior muscle tissue is typically larger and more prominent than the anterior side. In addition, the muscle tissue of the human lower limbs remained activated most of the time during the experiment. Therefore, in general, it is reasonable to conclude that k_{sfd-p} is larger than k_{sfd-n}.

V. Conclusion

This paper proposes a fractional-order human-exoskeleton coupling model with the segmented form (2) to represent the relationship between the human-exoskeleton relative movement and coupling force. Firstly, for the human-exoskeleton coupling, which includes components such as belt and human soft tissue, the fractional-order differential term is introduced to enhance the capability to characterize the mechanical characteristics of human-exoskeleton coupling. In addition, for the asymmetry of human-exoskeleton coupling, the segmented form is adopted for the differences in the mechanical characteristics of the front and back sides of the human-exoskeleton coupling point.

Based on the NFO and LS methods, the coupling parameters in (2) were then identified by a self-designed human-exoskeleton coupling measurement platform and with the help of 20 volunteers. By analyzing and discussing the results of model parameter identification, it is verified that the accuracy of the proposed fractional-order human-exoskeleton coupling model with the segmented form (2) is superior to that of the stiffness-damping model (1).

In future research work, we will utilize the model proposed in this paper to estimate the real-time human motion intention with coupling force in human-exoskeleton coupling motion control of the lower limb exoskeleton.

References

[1] R. Hidayah, L. Bishop, X. Jin, S. Chamarthy, J. Stein, and S. K. Agrawal, "Gait adaptation using a cable-driven active leg exoskeleton (c-alex) with post-stroke participants," *IEEE Transactions on Neural Systems and Rehabilitation Engineering*, vol. 28, no. 9, pp. 1984–1993, 2020.

[2] B. Koopman, E. H. Van Asseldonk, and H. Van Der Kooij, "Estimation of human hip and knee multi-joint dynamics using the lopes gait trainer," *IEEE Transactions on Robotics*, vol. 32, no. 4, pp. 920–932, 2016.

[3] K. N. Gregorczyk, L. Hasselquist, J. M. Schiffman, C. K. Bensel, J. P. Obusek, and D. J. Gutekunst, "Effects of a lower-body exoskeleton device on metabolic cost and gait biomechanics during load carriage," *Ergonomics*, vol. 53, no. 10, pp. 1263–1275, 2010.

[4] A. B. Zoss, H. Kazerooni, and A. Chu, "Biomechanical design of the berkeley lower extremity exoskeleton (bleex)," *IEEE/ASME Transactions on mechatronics*, vol. 11, no. 2, pp. 128–138, 2006.

[5] P. Asselin, C. M. Cirnigliaro, S. Kornfeld, S. Knezevic, R. Lackow, M. Elliott, W. A. Bauman, and A. M. Spungen, "Effect of exoskeletal-assisted walking on soft tissue body composition in persons with spinal cord injury," *Archives of physical medicine and rehabilitation*, vol. 102, no. 2, pp. 196–202, 2021.

[6] K. Miura, M. Koda, K. Tamaki, M. Ishida, A. Marushima, T. Funayama, H. Takahashi, H. Noguchi, K. Mataki, Y. Yasunaga *et al.*, "Exercise training using hybrid assistive limb (hal) lumbar type for locomotive syndrome: a pilot study," *BMC Musculoskeletal Disorders*, vol. 22, no. 1, p. 533, 2021.

[7] S. Oh, E. Baek, S.-k. Song, S. Mohammed, D. Jeon, and K. Kong, "A generalized control framework of assistive controllers and its application to lower limb exoskeletons," *Robotics and Autonomous Systems*, vol. 73, pp. 68–77, 2015.

[8] W. Meng, Q. Liu, Z. Zhou, Q. Ai, B. Sheng, and S. S. Xie, "Recent development of mechanisms and control strategies for robot-assisted lower limb rehabilitation," *Mechatronics*, vol. 31, pp. 132–145, 2015.

[9] M. S. Amiri, R. Ramli, and M. F. Ibrahim, "Hybrid design of pid controller for four dof lower limb exoskeleton," *Applied Mathematical Modelling*, vol. 72, pp. 17–27, 2019.

[10] G. Zhang, J. Wang, P. Yang, and S. Guo, "Iterative learning sliding mode control for output-constrained upper-limb exoskeleton with non-repetitive tasks," *Applied Mathematical Modelling*, vol. 97, pp. 366–380, 2021.

[11] Z. Chen, Q. Guo, Y. Yan, and Y. Shi, "Model identification and adaptive control of lower limb exoskeleton based on neighborhood field optimization," *Mechatronics*, vol. 81, p. 102699, 2022.

[12] C. Shen, Z. Pei, W. Chen, Z. Li, J. Wang, J. Zhang, and J. Chen, "Stmi: Stiffness estimation method based on semg-driven model for elbow joint," *IEEE Transactions on Instrumentation and Measurement*, vol. 77, p. 2526614, 2023.

[13] H. Van der Kooij, S. S. Fricke, R. C. vant Veld, A. V. Prieto, A. Q. Keemink, A. C. Schouten, and E. H. Van Asseldonk, "Identification of hip and knee joint impedance during the swing phase of walking," *IEEE Transactions on Neural Systems and Rehabilitation Engineering*, vol. 30, pp. 1203–1212, 2022.

[14] Y. Ma, Q. Liu, H. Liu, and W. Meng, "semg-based estimation of human arm endpoint stiffness using long short-term memory neural networks and autoencoders," in *International Conference on Intelligent Robotics and Applications*. Springer, 2022, pp. 699–710.

[15] Y. Liu, S. Guo, Z. Yang, H. Hirata, and T. Tamiya, "A home-based bilateral rehabilitation system with semg-based real-time variable stiffness," *IEEE Journal of Biomedical and Health Informatics*, vol. 25, no. 5, pp. 1529–1541, 2020.

[16] Y. Yan, Z. Chen, C. Huang, L. Chen, and Q. Guo, "Human-exoskeleton coupling dynamics in the swing of lower limb," *Applied Mathematical Modelling*, vol. 104, pp. 439–454, 2022.

[17] Y. Yan, Z. Chen, C. Huang, and Q. Guo, "Modelling and analysis of coupling dynamics of swinging a lower limb exoskeleton," *Nonlinear Dynamics*, vol. 111, no. 2, pp. 1213–1234, 2023.

[18] C. Huang, S. Ji, Z. Chen, T. Sun, Q. Guo, and Y. Yan, "Identification and analysis of human-exoskeleton coupling parameters in lower extremities," *IEEE Transactions on Haptics*, 2024.

[19] M. Ayyildiz, R. G. Aktas, and C. Basdogan, "Effect of solution and post-mortem time on mechanical and histological properties of liver during cold preservation," *Biorheology*, vol. 51, no. 1, pp. 47–70, 2014.

[20] Y. Aydin, O. Tokatli, V. Patoglu, and C. Basdogan, "Stable physical human-robot interaction using fractional order admittance control," *IEEE Transactions on Haptics*, vol. 11, no. 3, pp. 464–475, 2018.

[21] F. Mo, J. Li, M. Dan, T. Liu, and M. Behr, "Implementation of controlling strategy in a biomechanical lower limb model with active muscles for coupling multibody dynamics and finite element analysis," *Journal of biomechanics*, vol. 91, pp. 51–60, 2019.